

Minor trace gas radiative forcing calculations using the k distribution method with one-parameter scaling

David P. Kratz,¹ Ming-Dah Chou,² Michael M.-H. Yan,³ and Chang-Hoi Ho⁴

Abstract. The k distribution method with one-parameter pressure and temperature scaling, first developed for water vapor, has now been applied to the minor trace gas (N_2O , CH_4 , CFCs, and two minor bands of CO_2) absorption in the infrared window region (800–1380 cm^{-1}). The derivation of the k distributions is based upon an exponential sum fitting to the monochromatically calculated transmission functions at a predetermined reference pressure and temperature. For nonhomogeneous path lengths, one-parameter scaling is utilized in conjunction with the k distribution method. To determine the accuracies of the k distribution method as compared to the monochromatic calculations, fluxes and cooling rates are calculated for a wide variety of atmospheric conditions. For the entire 800–1380 cm^{-1} spectral range the effect of the minor trace gases on the fluxes calculated using the k distribution method is within 2.3% of the monochromatic method. In addition to being accurate, this method is computationally very fast. When implemented into the Goddard EOS general circulation model, the computing time for the longwave flux calculations is increased by only 20% despite the inclusion of the minor trace gas absorption bands.

1. Introduction

The thermal infrared energy emitted from the Earth-atmosphere system is characterized by a spectrum possessing a relatively transparent region known as the infrared window. Any molecular species which absorbs radiation within this region (7–12 μm) has the potential to significantly impact the radiation budget of the surface as well as the atmosphere. The most important molecular absorption features found within the infrared window are due to H_2O and O_3 . In addition, there is also the relatively weak but important absorption due to CO_2 in the 9.4 and 10.4 μm bands, as well as the absorption due to the minor trace gases N_2O , CH_4 , CFC-11, CFC-12, and HCFC-22. Recent studies [e.g., Wang *et al.*, 1991] have emphasized the importance of the radiative effects of these minor trace gases and that they should not be heuristically treated as simple equivalent amounts of CO_2 . Indeed, the radiative forcing of projected increases in the minor trace gases is estimated to be comparable to that of projected increases in CO_2 [Intergovernmental Panel on Climate Change (IPCC), 1995]. Nevertheless, it is important to realize that accounting for additional absorption within a radiative transfer model can result in significant increases to the

computing time. Thus efficient and accurate parameterizations are required for each of the minor trace gas absorption bands.

The present study is concerned with the development of these fast, accurate parameterizations for the trace gas absorption in the window region. To attain this goal, the present study utilizes the exponential sum fitting of transmission (ESFT) method to derive the k distributions from the transmission functions obtained through monochromatic calculations (both line-by-line and narrow spectral interval models). To be compatible with the study of Chou *et al.* [1993], the infrared window is taken from 800 to 1380 cm^{-1} . The monochromatic calculations used in this study are reviewed in section 2. The discussion then explains the basic philosophy supporting the k distribution method and the ESFT methodology used in deriving the k distribution function (section 3). To accommodate nonhomogeneous paths, the k distribution method is used in conjunction with the one-parameter scaling approximation. The present k distributions, when used with one-parameter scaling, allow for a substantial increase in the computational speed as compared with models using the usual correlated k distributions. This increased efficiency is very important for climate simulation studies that involve large numbers of radiative transfer calculations. In addition, unlike emissivity methods, the use of the k distribution method allows for multiple scattering calculations having a computational burden that is approximately linear (not quadratic) with the number of layers. The accuracy of the k distribution method is tested by comparing fluxes and cooling rates to those from the reference monochromatic calculations (section 4). With the accuracy of the k distribution method established, the new parameterizations are incorporated into

¹NASA Langley Research Center, Hampton, Virginia.

²NASA Goddard Space Flight Center, Greenbelt, Maryland.

³Science Systems & Application, Inc., Seabrook, Maryland.

⁴Department of Atmospheric Sciences, Seoul National University, Seoul, Korea

Copyright 1998 by the American Geophysical Union.

Paper number 1998JD200009.

0148-0227/98/1998JD200009\$09.00

the Goddard EOS (GEOS) general circulation model (GCM). The results of radiative forcing calculations using the GEOS GCM are presented in section 5.

2. The Line-by-Line/Monochromatic Method

The line-by-line, or monochromatic, method is the most rigorous approach for theoretically obtaining the absorption coefficient of a molecular species. The line-by-line derived absorption coefficient may be expressed as

$$k_{\omega}(p, \theta) = \sum_i S_i(\theta) f_{i,\omega}(p, \theta), \quad (1)$$

where ω is the wavenumber, p is the pressure, θ is the temperature, $S_i(\theta)$ is the intensity of the i th line, and $f_{i,\omega}(p, \theta)$ is the line shape factor assumed to have a Voigt profile. Each Voigt line is taken to have a line cutoff of 256 times the Lorentz half width or 5 times the Doppler half width, whichever is greater. Such a cutoff is incorporated both for computational efficiency and as an effective parameterization of the sub-Lorentzian nature of the far line wings [Fels and Schwarzkopf, 1981]. As a result of the current cutoff criteria, roughly 0.25% of the integrated intensity of the Voigt line is not included in the calculation.

The line locations, intensities, air-broadened Lorentz half widths, and lower state energies are taken from the 1992 version of the Air Force Geophysics Laboratory (AFGL) HITRAN database [Rothman et al., 1992]. The absorption coefficients have been computed with spectral resolutions of 0.005 cm^{-1} for all of the molecular species. The spectral resolutions chosen for the present study ensure accurate absorption calculations well into the stratosphere.

The chlorofluorocarbons, CFC-11, CFC-12, and HCFC-22, possess important absorption bands within the infrared window [Kratz et al., 1993; Clough and Iacono, 1995]. In the troposphere and stratosphere, however, the absorption bands of the CFC-11, CFC-12, and HCFC-22 are characterized by an extremely dense line structure with line spacings that are significantly smaller than the line half widths [Varanasi, 1992a,b], and the absorption coefficients are slowly varying functions of wavenumber [Penner, 1959]. Thus the use of the detailed line-by-line calculations is not warranted, and the laboratory-measured absorption coefficients can be used. For atmospheric modeling, Kratz and Varanasi [1992] concluded that a wavenumber resolution of 0.5 cm^{-1} is sufficient to yield band-integrated results that are virtually identical to those obtained at much finer resolutions. The present study uses the monochromatic method detailed by Kratz and Varanasi [1992] along with the laboratory measured absorption coefficients of Varanasi [1992a,b]. The CFC bands used in the present study are presented by Kratz et al. [1993, Table 1].

The monochromatic transmission (either the line-by-line or the fine spectral resolution method) may be integrated over a given spectral interval $\Delta\omega$, for a path length u , to yield the spectral-mean transmission

$$T_{\Delta\omega}(u, p, \theta) = \int_{\Delta\omega} \exp[-k_{\omega}(p, \theta)u] \frac{d\omega}{\Delta\omega}. \quad (2)$$

3. The k distribution Method and Exponential-Sum Fitting

For a narrow spectral interval and a homogeneous atmospheric layer (constant pressure and temperature), wavenumbers with the same absorption coefficient are radiatively equivalent and may be treated as one identity. Thus computational efficiency can be dramatically improved by substituting the integration over wavenumber by an integration over the absorption coefficient [see, e.g., Ambartsumian, 1936; Arking and Grossman, 1972]. The spectral-mean transmission from (2) can therefore be rewritten as

$$\begin{aligned} T_{\Delta\omega}(u, p, \theta) &= \int_0^{\infty} \exp[-k(p, \theta)u] h(k) dk \\ &= \int_0^1 \exp[-k_g(p, \theta)u] dg, \end{aligned} \quad (3)$$

where $h(k)$ is the probability distribution function of the k such that the fraction of the spectral interval with an absorption coefficient in the range from k to $k+dk$ is $h(k)dk$, and $g(k)$ is the cumulative probability function of k given by

$$g(k) = \int_0^k h(k') dk' \quad (4)$$

For calculations involving tropospheric and stratospheric pressures, Fu and Liou [1992] found that resolving the sharply peaked relationship between k and g required a g space resolution of order 0.001. While significant, the increase in computational speed afforded by the transformation from ω to g space, with a resolution of order 0.001, is still insufficient for use in climate model calculations. Further arbitrary reductions in the g space resolution may, however, compromise the accuracy of the model calculation. Thus it is necessary to apply a method whereby the optimal number of k values can be obtained for a specified accuracy, such as with the exponential sum fitting of transmissions (ESFT) method [see Kratz, 1995, references therein]. The ESFT method effectively replaces the spectral-mean transmission from (3) with a fit to a sum of exponentials

$$T_{\Delta\omega}(u, p, \theta) \approx \sum_{i=1}^N c_i \exp[-k_i(p, \theta)u]. \quad (5)$$

Thus the high spectral resolution calculated $T_{\Delta\omega}(u, p, \theta)$ is approximated by a summation over N monochromatic calculations corresponding to the absorption coefficients $k_i(p, \theta)$ and weights c_i . The physical interpretation of the terms $k_i(p, \theta)$ and c_i gives rise to the requirements that $k_i(p, \theta) \geq 0$, $c_i > 0$, and

$$\sum_{i=1}^N c_i = 1. \quad (6)$$

The ESFT method, detailed by Kratz [1995], is used to derive the coefficients c_i and $k_i(p, \theta)$ in (5). In this ESFT method the values of $k_i(p, \theta)$ are selected a priori to be constrained by the relationship

$$k_i(p, \theta) = nk_{i-1}(p, \theta), \quad (7)$$

Table 1. Coefficients for the Transmission Functions Attributed to the Molecular Absorption of H₂O, O₃, and CO₂ That Were Not Previously Considered by *Chou et al.* [1993] in the Spectral Range From 800 to 1380 cm⁻¹

Band	H ₂ O		O ₃		CO ₂	
	1100–1215	1215–1380	800–980	1100–1215	800–980	980–1100
k_1	5.385X10 ⁻³	2.843X10 ⁻²	1.247	11.00	5.993X10 ⁻³	1.306X10 ⁻²
n	8	9		164	60	44
c_1	0.595478	0.195768	1.0	0.991419	0.972025	0.961324
c_2	0.269246	0.346907		0.008581	0.027975	0.038676
c_3	0.095317	0.314672				
c_4	0.033524	0.101340				
c_5	0.006435	0.036548				
c_6		0.004765				
m	0.77	0.50	0	0.14	0	0
a	1.91X10 ⁻²	1.52X10 ⁻²	2.69X10 ⁻²	2.61X10 ⁻³	3.58X10 ⁻²	3.43X10 ⁻²
b	1.11X10 ⁻⁴	7.61X10 ⁻⁵	2.71X10 ⁻⁴	7.70X10 ⁻⁶	4.04X10 ⁻⁴	3.74X10 ⁻⁴
r	1.66	1.66	2.00	1.83	1.83	1.83

Here k_1 is the first absorption coefficient (cm² g⁻¹), n is the constant where $k_i = n k_{i-1}$, c_i are the weights, m is the pressure scaling exponent, a and b are the temperature correction coefficients, r is the diffusivity factor, and θ_{ref} equals 250 K and P_{ref} equals 500 hpa, except O₃ where P_{ref} equals 100 hpa. For CO₂ absorption in the 800–980 cm⁻¹ range, m equals 0.16 for $P > P_{ref}$, while in the 980–1100 cm⁻¹ range, m equals 0.24 for $P > P_{ref}$.

where n is a positive integer. Thus each of the exponential terms is derived from the previous $k_i(p, \theta)$.

To accommodate the various minor trace gas absorption bands, the 800–1380 cm⁻¹ spectral range is divided into four intervals. Two of the intervals (800–980 and 980–1100 cm⁻¹) correspond directly with those of *Chou et al.* [1993]. The highly nonuniform nature of the minor trace gas absorption within the 1100–1380 cm⁻¹ interval, however, necessitates dividing that interval into two subintervals (1100–1215 and 1215–1380 cm⁻¹). In addition to minor trace gas k distributions that have been made for all four intervals, k distributions are also computed for the O₃ absorption in the 800–980 and 1100–1215 cm⁻¹ intervals.

Furthermore, the subdivision of the 1100–1380 cm⁻¹ interval necessitated computing k distributions for the H₂O absorption found in these subintervals. The first value of k , n , and the weights for the absorption bands within the four spectral intervals are presented in Tables 1–3. For completeness, a set of k distribution coefficients was also computed for the N₂O absorption in the 540–620 cm⁻¹ spectral range and is presented in Table 2. The k distributions for the absorption due to H₂O in the 800–980 and 980–1100 cm⁻¹ intervals and the absorption due to O₃ in the 980–1100 cm⁻¹ interval are reported by *Chou et al.*, [1993] and *Chou and Kouvaris* [1991].

The CFC absorption bands involve spectral ranges

Table 2. Same as Table 1 Except for N₂O and CH₄

Band	N ₂ O			CH ₄	
	540–620	1100–1215	1215–1380	1100–1215	1215–1380
k_1	69.45	16.93	15.95	4.065	51.22
n	58	21	8		12
c_1	0.970831	0.940414	0.561961	1.0	0.610650
c_2	0.029169	0.059586	0.138707		0.280212
c_3			0.240670		0.107349
c_4			0.058662		0.001789
m	0	0	0.48	0	0.65
a	1.45X10 ⁻³	1.93X10 ⁻³	1.38X10 ⁻³	1.70X10 ⁻²	5.96X10 ⁻⁴
b	3.67X10 ⁻⁶	4.37X10 ⁻⁶	7.48X10 ⁻⁶	1.58X10 ⁻⁴	-2.29X10 ⁻⁶
r	1.83	1.83	1.66	2.00	1.66

For N₂O absorption in the 540–620 cm⁻¹ range, m equals 0.33 for $P > P_{ref}$.

Table 3. Same as Table 1 Except for CFC-11, CFC-12 and HCFC-22

Band	CFC-11		CFC-12		HCFC-12	
	800–980	980–1100	800–980	1100–1215	800–980	1100–1215
k	$1.547 \times 10^{+3}$	$8.275 \times 10^{+2}$	$1.465 \times 10^{+3}$	$3.428 \times 10^{+3}$	$8.012 \times 10^{+2}$	$4.247 \times 10^{+3}$
c	1.0	1.0	1.0	1.0	1.0	1.0
m	0	0	0	0	0	0
a	1.27×10^{-3}	8.19×10^{-4}	8.77×10^{-4}	8.62×10^{-4}	9.65×10^{-4}	-3.00×10^{-5}
b	3.56×10^{-6}	4.68×10^{-6}	-5.88×10^{-6}	-4.23×10^{-6}	1.31×10^{-5}	5.25×10^{-7}
r	2.00	2.00	2.00	2.00	2.00	2.00

These CFCs are taken to be in the optically thin limit and are modeled with a single k coefficient.

which do not correspond precisely with the spectral intervals presented in Table 3. The method used to account for this spectral mismatch takes advantage of the observation that calculations using the current or projected CFC abundances [IPCC, 1995] yield band absorptances close to the linear regime of the curve of growth where $(1 - \exp(-k_\omega u)) \approx k_\omega u$. For an optically thin absorption band spanning the spectral range from ω_a to ω_b , the emission of a layer with temperature θ can be written as

$$E = \int_{\omega_a}^{\omega_b} k_\omega(\theta) u B_\omega(\theta) d\omega, \quad (8)$$

where $B_\omega(\theta)$ is the Planck function value at wavenumber ω . Note that the interval of ω_a to ω_b represents the entire range of an absorption band of a trace gas [see Kratz *et al.* 1993, Table 1], while ω_1 and ω_2 are the boundaries of the spectral band used in the radiation model where the trace gas absorption band is located (see Tables 1–3). The effective emission of this absorption band for a model's prescribed spectral range which runs from ω_1 to ω_2 (see Table 3) can be written as

$$E_{\text{eff}} = \int_{\omega_1}^{\omega_2} \bar{k}(\theta) u B_\omega(\theta) d\omega, \quad (9)$$

where \bar{k} is the effective absorption coefficient for the CFC band. By equating (8) and (9), \bar{k} can be determined

$$\bar{k}(\theta) = \int_{\omega_a}^{\omega_b} k_\omega(\theta) B_\omega(\theta) d\omega / \int_{\omega_1}^{\omega_2} B_\omega(\theta) d\omega. \quad (10)$$

The results from this method have proven to be very accurate when compared to high spectral resolution calculations. Indeed, the accuracies are comparable to those of parameterizations using more k values and explicitly considering any spectral mismatch. The k distribution coefficients obtained for the CFCs by this method are presented in Table 3.

As with any parameterized radiation model, the k distribution method requires some approximations to accommodate the nonhomogeneity of the atmosphere. One such approximation is to scale the nonhomogeneous path to an equivalent homogeneous path. While several different scaling methods have been devised, a particularly efficient yet accurate one is the one-parameter wing-scaling approximation [Chou *et al.*, 1993]. For the wing-scaling

approximation the absorption coefficient is related to the absorption coefficient at the reference pressure p_r and temperature θ_r by

$$k_i(p, \theta) = k_i(p_r, \theta_r) (p/p_r)^m s(\theta, \theta_r), \quad (11)$$

where m is a positive value number between 0 and 1 and $s(\theta, \theta_r)$ is the temperature-scaling function. In the current study, the pressure-scaling coefficient, m , in (11) is empirically determined to minimize the flux errors between the pressures of 10 and 1000 hPa at a reference temperature ($\theta_r = 250$ K). The results are presented in Tables 1–3. The pressure-scaling coefficient is taken to be zero for several of the absorption bands because either the absorption is nearly in the linear regime of the curve of growth or the pressure dependence is sufficiently weak that little benefit is obtained by considering the effect of pressure on k . The temperature dependent scaling function, $s(\theta, \theta_r)$ in (11), is given by

$$s(\theta, \theta_r) = 1.0 + a(\theta - \theta_r) + b(\theta - \theta_r)^2. \quad (12)$$

The derived values for the coefficients a and b are also presented in Tables 1–3. Note that the coefficients a and b are independent of pressure and k_i . By applying the scaling formulation in (11), the dependence of k on wavenumber is separated from the dependence of k on pressure and temperature. Thus, whenever absorption coefficients within a wavenumber interval are determined to have equal values at the reference pressure and temperature, the absorption coefficients can be taken to have equal values at any pressure and temperature. Since these absorption coefficients can be treated identically, the k distribution can be applied to a nonhomogeneous path. For a nonhomogeneous layer between altitudes z' and z'' , (5) is reduced to

$$T_{\Delta\omega}(z', z'') \approx \sum_{i=1}^N c_i \exp[-k_i(p_r, \theta_r) u_s(z', z'')], \quad (13)$$

where u_s is the scaled absorber amount given by

$$u_s(z', z'') = \int_{z'}^{z''} (p/p_r)^m s(\theta, \theta_r) \rho dz \quad (14)$$

and ρ is the density of the absorber. Thus the scaling of k is reduced to a scaling of u .

It is important to note that the $k_i(p, \theta)$ relationship in (7) allows for a substantial increase in computational speed when the k distribution is used in conjunction with the one-parameter scaling approximation given in (11). The increased computational speed is associated with the fact that only the first k value needs to be computed with an exponential operation. All subsequent terms can be derived from the previous value of k using multiplication operations which tend to be significantly faster than exponential operations [Chou *et al.*, 1993]. Because the individual pressure and temperature dependences of the k values are retained in correlated k distribution routines, models such as *Lacis and Oinas* [1991] and *Fu and Liou* [1992] are unable to take advantage of this computational enhancement. The efficiency of a model, however, is critical for climate simulation studies that involve large numbers of radiative transfer calculations.

As noted by Chou *et al.* [1993], since $k_i(p, \theta)$ is extrapolated from $k_i(p, \theta_s)$, the one-parameter scaling approximation is most accurate for pressures and temperatures close to their reference values. For most of the absorption bands considered in the current study, one-parameter scaling works quite well because the bulk of the absorption is confined to the lower reaches of the atmosphere. Thus, with a judicious selection of the reference pressures and temperatures, highly accurate flux calculations can be obtained throughout the Earth's atmosphere.

The molecular absorption within the 800–1380 cm^{-1} spectral range arises from a combination of overlapping absorption from several molecular species. To account for the overlap of absorption due to the different molecular species, we make use of the multiplication rule [Goody and Yung, 1989], which inherently assumes that the spectral absorptions of the different molecular species are uncorrelated with one another. The spectral mean transmittance for the combination of any two different molecular species is thereby given by

$$T_{\Delta\omega}^{\text{total}} \approx T_{\Delta\omega}^1 T_{\Delta\omega}^2 \quad (15)$$

where $T_{\Delta\omega}^{\text{total}}$ is the transmission due to the two gases taken together, while $T_{\Delta\omega}^1$ and $T_{\Delta\omega}^2$ are the transmissions due to the gases taken separately.

4. Atmospheric Flux and Cooling Rate Calculations

A determination of the accuracies of the present k distributions is made by comparing fluxes as calculated using the k distribution method and reference monochromatic routines. The pressures, temperatures, and H_2O and O_3 abundances are taken to follow the atmospheric profiles from updated versions of the *McClatchey et al.* [1972] profiles as reported by *Ellingson et al.* [1991]. The vertical spacings within the atmospheres were taken to be 1 km from the surface to 25 km, and 5 km from 25 km to the top of the atmosphere (70 km). Since the focus is on the radiative effects of molecular absorption for the clear-sky case, we do not consider the radiative effects of clouds and aerosol layers. The minor trace gases have been taken to have the following mixing ratios which correspond

closely to the 1992 abundances [IPCC, 1995]. These values are 350 ppmv for CO_2 , 310 ppbv for N_2O , 1.75 ppmv for CH_4 , 0.268 ppbv for CFC-11, 0.503 ppbv for CFC-12, and 0.105 ppbv for HCFC-22.

The net upward flux $F_{\Delta\omega}(z)$ for the wavenumber interval $\Delta\omega$ at altitude z may be written as

$$F_{\Delta\omega}(z) = 2\pi B_{\Delta\omega}(\theta_s) \int_0^1 T_{\Delta\omega}[z; \mu] \mu d\mu \\ + 2\pi \int_0^1 \int_0^{z_\infty} B_{\Delta\omega}(\theta) dT_{\Delta\omega}[z'; z; \mu] \mu d\mu. \quad (16)$$

The terms in (16) not previously defined include the spectrally integrated Planck function $B_{\Delta\omega}$, the surface temperature θ_s , the altitude taken for the top of the atmosphere z_∞ , the altitude integration variable z' , and the cosine of the zenith angle μ . To accomplish the angular integration for diffuse transmission, the line-by-line (or high spectral resolution) method used an eight-point Gaussian quadrature; the k distribution method used both an eight-point Gaussian quadrature and the diffusivity approximation. The values used in the diffusivity approximation are taken to be 1.66 ~ 5/3 for bands that have optically thick absorption lines, 2.0 for bands that are optically thin, and 1.83 ~ 11/6 for intermediate cases. The diffusivity values are given in Tables 1–3.

Model calculations are presented in Tables 4 and 5 for the reduction in the upward radiative flux to the top of the atmosphere ($\Delta F_{\text{toa}}^\uparrow$), and the enhancement to the downward radiative flux at the surface ($\Delta F_{\text{surf}}^\downarrow$). The results in Table 4, which consider the radiative effects of the individual molecular species, are reported for the *McClatchey et al.* [1972] midlatitude summer (MLS) atmosphere. For Table 5 the fluxes are reported for the *McClatchey et al.* [1972] MLS atmosphere as well as the tropical (TRO) and midlatitude winter (MLW) atmospheres for the case where the radiative effects of the minor trace species including the weak bands of CO_2 are taken together for the entire 800–1380 cm^{-1} spectral interval. Overlapping with H_2O and O_3 absorption is excluded.

The radiative forcings attributed to H_2O (lines only) are presented in Table 4 for the spectral intervals of 1100–1215 and 1215–1380 cm^{-1} . Chou *et al.* [1993] had previously presented k distributions for H_2O for the 800–980 and 980–1100 cm^{-1} spectral ranges. The k distribution method for the H_2O yields results within about 2% of those of the line-by-line method. The radiative forcings attributed to O_3 are also presented in Table 4 for the spectral intervals of 800–980 and 1100–1250 cm^{-1} . Percentage errors are somewhat worse for O_3 , approaching 10%. Much of the observed discrepancy arises from the difficulty of applying scaling to O_3 . This difficulty is due to the vertical distribution of O_3 , which has relatively small concentrations in the troposphere where temperatures are high and pressure broadening is quite strong, and relatively high concentrations in the stratosphere where the temperatures are low and pressure broadening is much weaker.

The radiative forcings attributed to the separate occurrences of the minor trace gases CO_2 , N_2O , CH_4 , CFC-11, CFC-12, and HCFC-22 are also presented in Table 4. For CO_2 , N_2O , and CH_4 the k distribution routines using one-parameter scaling are compared to the

Table 4. Radiative Forcings Due to the Separate Occurrences of H₂O, O₃, CO₂, N₂O, CH₄, CFC-11, CFC-12, and HCFC-22

Gases	Spectral Range	Model	$\Delta F_{\text{toa}}^{\uparrow}$	$\Delta F_{\text{sfc}}^{\downarrow}$
H ₂ O	1100–1215	line-by-line	1.583	6.380
		<i>k</i> (<i>P</i> -scaled)	1.549	6.294
	1215–1380	line-by-line	7.935	18.193
		<i>k</i> (<i>P</i> -scaled)	8.043	18.126
O ₃	800–980	line-by-line	0.042	0.027
		<i>k</i> (<i>P</i> -scaled)	0.041	0.029
	1100–1215	line-by-line	0.457	0.149
		<i>k</i> (<i>P</i> -scaled)	0.443	0.161
CO ₂	800–980	line-by-line	0.372	1.092
		<i>k</i> (<i>P</i> -scaled)	0.363	1.109
	980–1100	line-by-line	0.423	1.069
		<i>k</i> (<i>P</i> -scaled)	0.423	1.095
N ₂ O	540–620	line-by-line	1.198	2.588
		<i>k</i> (<i>P</i> -scaled)	1.229	2.590
	1100–1215	line-by-line	0.357	0.418
		<i>k</i> (<i>P</i> -scaled)	0.358	0.407
	1215–1380	line-by-line	2.836	3.759
		<i>k</i> (<i>P</i> -scaled)	2.797	3.665
CH ₄	1100–1215	line-by-line	0.087	0.149
		<i>k</i> (<i>P</i> -scaled)	0.087	0.150
	1215–1380	line-by-line	4.572	6.103
		<i>k</i> (<i>P</i> -scaled)	4.590	6.117
CFC-11	800–980	monochromatic	0.090	0.155
		<i>k</i> distribution	0.088	0.145
	980–1100	monochromatic	0.027	0.037
		<i>k</i> distribution	0.026	0.037
CFC-12	800–980	monochromatic	0.147	0.223
		<i>k</i> distribution	0.142	0.224
	1100–1215	monochromatic	0.142	0.178
		<i>k</i> distribution	0.144	0.176
HCFC-22	800–980	monochromatic	0.011	0.019
		<i>k</i> distribution	0.011	0.019
	1100–1215	monochromatic	0.025	0.033
		<i>k</i> distribution	0.026	0.032

$\Delta F_{\text{toa}}^{\uparrow}$ is the reduction in the upward flux at the top of the atmosphere (toa), and $\Delta F_{\text{sfc}}^{\downarrow}$ is the enhancement to the downward flux at the surface (sfc). The fluxes are in W m^{-2} , and are computed using an eight-point gaussian quadrature. The spectral range is in cm^{-1} . The atmospheric profile is taken to be the McClatchey *et al.* [1972] midlatitude summer (MLS) atmosphere.

reference line-by-line method. The agreement between the *k* distribution and the reference line-by-line flux calculations is within 2.5% for CO₂ and N₂O and 0.5% for CH₄. For the CFCs the single *k* calculations are compared to the narrow-interval (0.5 cm^{-1}) monochromatic method. As with H₂O and the other minor trace gases, the results of the CFC *k* distribution calculations lie within several percent of the reference monochromatic flux calculations.

Table 5 summarizes the radiative forcing attributed to the absorption bands of the minor trace species (CO₂, N₂O,

CH₄, and the CFCs) for the 800–1380 cm^{-1} interval, as well as the absorption band of N₂O for the 540–620 cm^{-1} interval. The results in Table 5 illustrate that the *k* distribution with one-parameter scaling yields results within 2.3% of the reference line-by-line method for a variety of atmospheric conditions. When overlapping with H₂O and O₃ is included, the flux calculations using the *k* distribution with one-parameter scaling yields results within 1.3% of the reference line-by-line method (not shown in Table 5). An intercomparison of the *k*

Table 5. Radiative Forcing Due to the Minor Trace Gases (Excluding H₂O and O₃) Listed in Tables 1-3 for the Entire 800-1380 cm⁻¹ Spectral Interval

Atmosphere	Model	Quadrature	$\Delta F_{\text{toa}}^{\uparrow}$	$\Delta F_{\text{sfc}}^{\downarrow}$
TRO	line-by-line	8-point	9.715	12.971
	k (P -scaled)	8-point	9.917	13.264
	k (P -scaled)	diffuse	9.838	13.222
MLS	line-by-line	8-point	8.102	11.730
	k (P -scaled)	8-point	8.277	11.998
	k (P -scaled)	diffuse	8.208	11.959
SAW	line-by-line	8-point	2.466	5.107
	k (P -scaled)	8-point	2.508	5.195
	k (P -scaled)	diffuse	2.474	5.169

$\Delta F_{\text{toa}}^{\uparrow}$ is the reduction in the upward flux at the top of the atmosphere (toa), and $\Delta F_{\text{sfc}}^{\downarrow}$ is the enhancement to the downward flux at the surface (sfc). The fluxes are in W m⁻², and are computed using both an eight-point gaussian quadrature and a diffusivity approximation. The spectral range is in cm⁻¹. The McClatchey *et al.* (1972) tropical (TRO), midlatitude summer (MLS), and subarctic winter (SAW) atmospheres are used.

distribution results using the eight-point Gaussian quadrature and the diffusivity approximation demonstrates the soundness of the present diffusivity approximation.

The cooling rate of a layer with a thickness Δp in the spectral interval is given by

$$\frac{\Delta\theta}{\Delta t} = -\frac{g_e}{C_p} \frac{\Delta F_{\Delta\omega}}{\Delta p}, \quad (17)$$

where g_e is the gravitational acceleration and C_p is the specific heat at constant pressure. Figure 1a illustrates the cooling rate in the 800–1380 cm⁻¹ spectral range for the minor trace gases (CO₂, N₂O, CH₄, CFC-11, CFC-12, and HCFC-22) in an atmosphere without any other absorbers.

To a first approximation, near the surface, the relatively warm minor trace gases have a net absorption of energy from the higher-temperature surface and a net emission of energy to space. Since the net emission to space is greater, the effect of the trace gases is to cool the lowest few kilometers of the atmosphere. Near the tropopause the relatively cool minor trace gases still have a net absorption of energy from the surface and a net emission of energy to space; however, more energy is absorbed by the layers near the tropopause than is emitted, and thus the effect of the trace gases is to warm the upper troposphere and lower stratosphere. Higher in the stratosphere, where the temperatures again rise, the minor trace gases once again

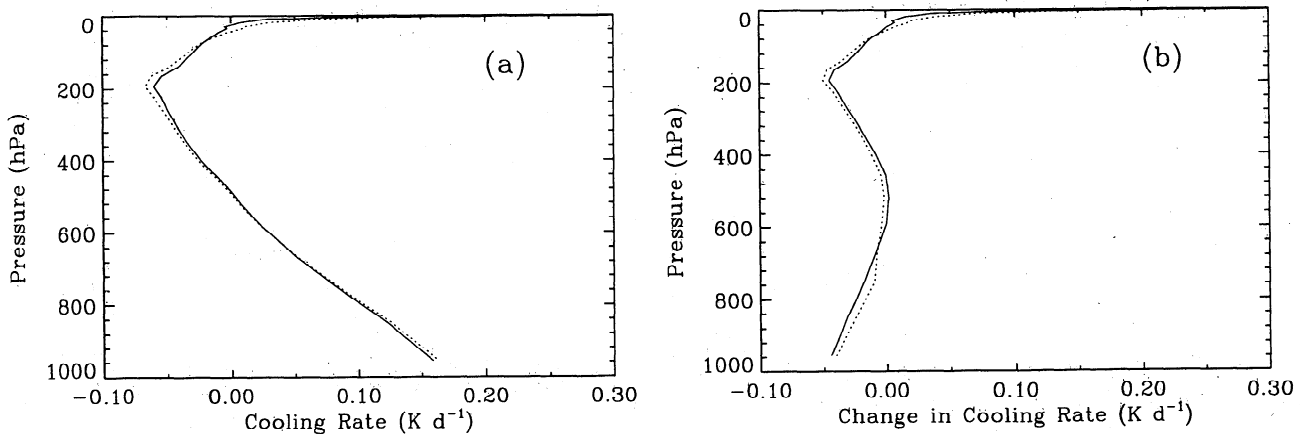


Figure 1. Cooling rate profiles for the minor absorption bands (CO₂, N₂O, CH₄, CFC-11, CFC-12, and HCFC-22) calculated from the reference line-by-line/monochromatic method (solid curves) and the k distribution (dashed curves). The calculated values represent the cooling rates for the spectral range from 800 to 1380 cm⁻¹ for the McClatchey *et al.* [1972] midlatitude summer atmosphere. Figure 1a represents the cooling rates resulting from the introduction of the minor trace gases into an atmosphere where no other absorber is considered. Figure 1b represents the change in the cooling rates resulting from the introduction of the minor trace gases into an atmosphere already containing H₂O and O₃.

emit more energy than they absorb and hence cool the upper stratosphere.

Figure 1b illustrates the change in the cooling rates due to the introduction of the minor trace gases into an atmosphere already containing H_2O and O_3 . Because H_2O absorption causes the lower troposphere to be relatively opaque in the $1215\text{--}1380\text{ cm}^{-1}$ spectral range, where much of the minor trace gas absorption occurs (see, e.g., Table 4), the addition of the minor trace gases decreases the lower troposphere's ability to cool to space. Thus the impact of including the minor trace gases into an atmosphere already containing H_2O and O_3 is to reduce the cooling rate in the lower troposphere. Higher in the atmosphere where the H_2O absorption is relatively thin, the minor trace gas induced changes to the cooling rates are far less dependent upon the presence of H_2O (compare Figures 1a and 1b). Wang *et al.* [1991] reported similar results for the minor trace gas cooling rates in their Figure 3a.

5. Implementation Into the GEOS GCM

Because of the numerous trace gas absorption bands involved, incorporation of these bands in a longwave model has the potential to be very expensive, especially for long-term integration of a numerical model for climate studies. For the prediction of future greenhouse warming the climate response to the radiative forcing due to CO_2 has been used as a proxy for that due to the minor trace gases. The vertical distribution of the radiative forcing due to CO_2 , however, is very different from that due to the minor trace gases. Thus the use of the CO_2 proxy has the potential to lead to serious errors. In experiments with the National Center for Atmospheric Research (NCAR) GCM, Wang *et al.* [1991] discovered that while the CO_2 proxy can be used for assessing the response of global-mean surface temperature, it cannot be used for regional climate. Discrepancies greater than 10% in the response of the surface temperature caused by the CO_2 proxy have been found in some continental regions. Thus it is important to explicitly include the absorption due to minor trace gases in GCM climate studies.

We have incorporated the k distribution method with one-parameter pressure scaling for the minor trace gas absorption bands into the GEOS GCM. The spectral bands and absorbers now considered by the GEOS GCM are given in Table 1 of Chou and Suarez [1994] along with Tables 1–3 of the present study. Even with the addition of the spectral bands for the minor trace gases, the computing time for longwave radiation increases by only 20%, indicating the efficiency of the new parameterization. Note that a k distribution routine which accounts for the $17\text{ }\mu\text{m}$ band of N_2O , while only briefly mentioned here, has also been incorporated into the GEOS GCM within the spectral interval $540\text{--}620\text{ cm}^{-1}$. Using the GEOS GCM simulations of temperature, humidity, and cloud fields, off-line calculations of the radiative forcing due to these minor bands were performed for each month and averaged to derive global and annual mean radiative forcing. The radiative forcing, or, more precisely, the instantaneous radiative forcing, is defined as the effect on the radiation budgets due to changes in only the minor trace gases with no feedback between radiation and climate. To assess the

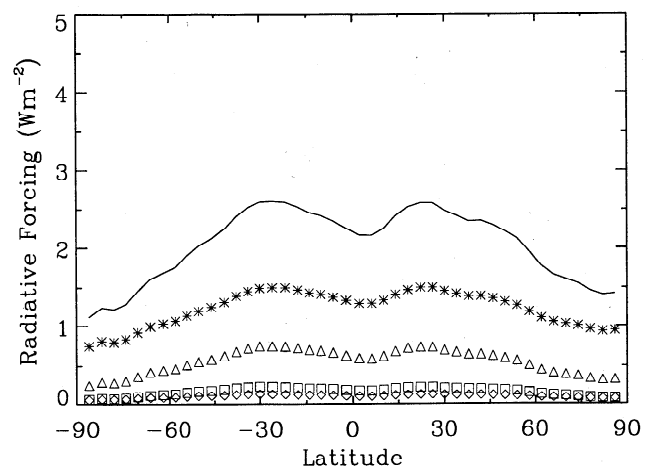


Figure 2. Latitudinal distributions of radiative forcing at the tropopause due to changes in the atmospheric concentrations of the minor trace gases since the preindustrial era. The solid curve represents the total forcing attributed to anthropogenic activities, while the symbol curves represent the contributions from the CO_2 ($15\text{ }\mu\text{m}$ + minor bands) (asterisks), CH_4 (triangles), N_2O (diamonds), and the CFCs (squares). A positive forcing implies a decrease in the net upward flux.

anthropogenic effect on the Earth's radiation budgets, the radiative forcing due to changes in CO_2 , CH_4 , N_2O , and CFCs from the preindustrial era is computed. The results are shown in Figure 2 for the latitudinal distributions of the radiative forcing at the tropopause ($\approx 200\text{ hPa}$) due to CO_2 , CH_4 , N_2O , and CFCs, as well as the total forcing of these gases. The forcing is with respect to the change from the preindustrial value of 280 ppmv to the present value of 350 ppmv for CO_2 , from 0.7 to 1.75 ppmv for CH_4 , from 0.275 to 0.311 ppmv for N_2O , from 0 to 0.268 ppbv for CFC-11, from 0 to 0.503 ppbv for CFC-12, and from 0 to 0.105 ppbv for HCFC-22. As expected, CO_2 has the largest impact on the Earth's radiation budget. While not the primary focus of the present study, the CO_2 calculations do provide a reference upon which to compare the minor trace gas radiative forcing and climate response calculations. The CH_4 forcing is nearly half of the CO_2 forcing. The radiative forcings due to anthropogenic increases of N_2O and CFCs are small. The latitudinal distributions of all the forcings are similar. The relative minimum in the equatorial region is due to both large cloud amounts (relative to the subtropics) and high cloud top altitudes. The minimum in the polar regions is due to both relatively large cloud amounts and the small temperature lapse rate. Since most clouds are very opaque in the thermal infrared, the amount and altitude are the most important cloud parameters affecting the calculations of radiative forcing due to minor trace gases. The radiative forcing decreases as both cloud amount and height increase. In the extreme case of an isothermal atmosphere the outgoing longwave radiation is independent of CO_2 and trace gas amount. Hence the radiative forcing of greenhouse gases depends not only on the amount of the gases but also on the lapse rate of the atmospheric temperature. Table 6 shows the global mean radiative

Table 6. Global Mean Radiative Forcing Due to Changes in the Atmospheric Concentrations of the Minor Trace Gases Since the Preindustrial Era

Molecular Species	TOA	Tropopause	Surface
CO ₂	0.81	1.32	0.30
CH ₄	0.65	0.62	0.24
N ₂ O	0.11	0.11	0.03
CFC	0.24	0.18	0.14
CO ₂ +CH ₄ +N ₂ O+CFC	1.83	2.24	0.71

The fluxes are in W m⁻².

forcing due to these gases at the top of the atmosphere, the tropopause, and the surface. The total anthropogenic forcing at the tropopause, which is the dominate parameter controlling the response of the global surface temperature, is 2.2 W m⁻². Over 85% of this forcing comes from increases in CO₂ and CH₄. The small forcing of 0.11 W m⁻² due to N₂O is attributable to the small change in its concentration in the atmosphere, from 0.275 to 0.310 ppmv. The overall forcing of 2.2 W m⁻² is comparable to the instantaneous radiative forcings at the tropopause of 2.1 W m⁻² reported by *Kiehl and Briegleb* [1993] and 2.3 W m⁻² reported by *Shi and Fan* [1992]. The present instantaneous forcing, however, is about 10% less than the adjusted radiative forcing estimated by the *IPCC* [1995]. The differences between our results and the *IPCC's* [1995] cannot be reconciled by accounting for the difference between our use of an instantaneous forcing, where stratospheric temperatures remain unaltered, and their use of an adjusted forcing, where stratospheric temperatures are allowed to readjust to the instantaneous forcing. Although the most important factor affecting the radiative

Table 7. Global Mean Radiative Forcing Due to the Minor Trace Gases at Their Present (circa 1992) Atmospheric Concentrations

Molecular Species	TOA	Tropopause	Surface
CO ₂ (minor bands)	0.31	0.33	0.49
CH ₄	1.82	1.65	0.73
N ₂ O	1.59	1.45	0.52
CFC	0.24	0.18	0.14
CO ₂ +CH ₄ +N ₂ O+CFC	3.75	3.44	1.77

The fluxes are in W m⁻².

forcing calculations is the radiation model, the various models use different temperature and humidity profiles and, most importantly, different cloud distributions and types. Thus, without detailed knowledge of the model inputs, it is not possible to trace the sources of the difference in radiative forcing calculations.

The radiative effect of neglecting these minor absorption bands in the GEOS GCM simulations for the current climate is shown in Figure 3 and Table 7. These results show the difference between the radiative fluxes computed with and without the current level of these minor trace gases. These off-line calculations of radiative fluxes do not have feedback between radiation and climate. It can be seen that the total effect of neglecting these gases is to enhance the net upward longwave radiation at the tropopause by 3.4 W m⁻², which is comparable to the forcing of a doubling of the atmospheric CO₂. Most of the minor trace gas effect is due to CH₄ and N₂O. The contribution of the two minor CO₂ bands is smaller, being about 10% of the total.

6. Summary and Conclusions

It has become increasingly evident that simulations of the potential climatic changes due to anthropogenic activities require a model which considers the radiative effects of the minor trace gases. We have therefore developed fast, accurate parameterizations for the molecular absorption in the infrared window region located between 800 and 1380 cm⁻¹. The parameterization uses the *k* distribution method, which is based upon a transformation of the distribution of the absorption coefficients from wavenumber space to cumulative probability space. To maximize the efficiency, an ESFT procedure has been applied to derive the *k* distributions. To account for nonhomogeneous path lengths, a one-parameter scaling method has been applied. When all of the minor trace species in the present study are considered for the entire 800–1380 cm⁻¹ spectral range, the *k* distribution with one-parameter scaling yields radiative forcing flux calculation results within 2.3% of the monochromatic method. In addition, for *p* > 30 hPa, the cooling rates from the *k* distribution model agree to within 0.01 K d⁻¹ of the cooling rates from the monochromatic calculations for both the cases with and without overlapping by H₂O and O₃. The impact of introducing the minor trace species into an atmosphere with H₂O and O₃ is to reduce the total

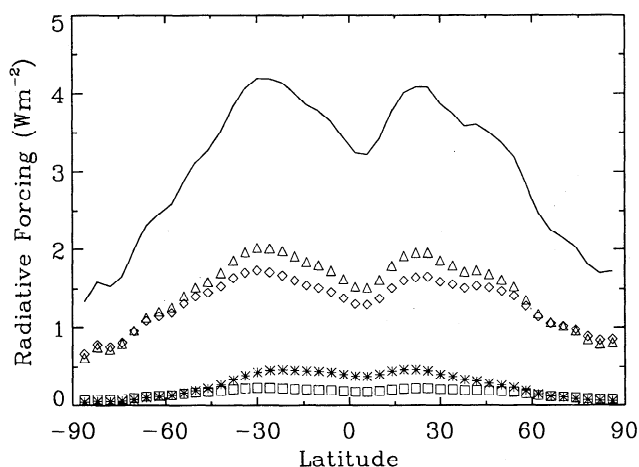


Figure 3. Latitudinal distributions of radiative forcing at the tropopause due to minor absorption bands with the present level of the atmospheric trace gas concentrations. The solid curve represents the total forcing attributed to all the minor trace species, while the symbol curves represent the contributions from the CO₂ (minor bands only) (asterisks), CH₄ (triangles), N₂O (diamonds), and the CFCs (squares).

cooling rate both in the lower troposphere and near the tropopause. With the accuracies of the k distribution routines established, the new parameterizations have been efficiently incorporated into the GEOS GCM to investigate the radiative forcings due to CO₂, CH₄, N₂O, and several of the CFCs.

In addition to being accurate and fast, the k distribution method has also proven to be highly versatile. For instance, recent studies [e.g., Prabhakara et al., 1993] have emphasized the significance of scattering of radiation in the infrared window region by cirrus clouds. Indeed, as can be seen in Figure 2 of Prabhakara et al. [1993], the assumption of gray-body emission by cirrus clouds is not valid. Since the k distribution method, unlike many other parameterizations, can be used for media that both scatter and absorb, it is applicable to radiative transfer calculations that involve clouds [e.g., Stackhouse and Stephens, 1991]. Moreover, because the infrared window region is subdivided into four intervals, some accommodation for the variation in the cloud optical properties can be made.

Acknowledgments. The authors would like to thank G. Gibson, T. P. Charlock, and the reviewers for their helpful comments concerning the manuscript. The authors would also like to thank A. C. Wilber for her assistance in preparing the manuscript for publication. The work at Langley was supported by the NASA Earth Observing System Program. The work at Goddard was supported by the NASA Global Modeling and Analysis Program.

References

- Ambartzumian, V., The effect of the absorption lines on the radiative equilibrium of the outer layers of the stars, *Publ. Obs. Astron. Univ. Leningrad.*, 6, 7–18, 1936.
- Arking, A., and K. Grossman, The influence of line shape and band structure on temperatures in planetary atmospheres, *J. Atmos. Sci.*, 29, 937–949, 1972.
- Chou, M.-D., and L. Kouvaris, Calculations of transmission functions in the IR CO₂ and O₃ bands, *J. Geophys. Res.*, 96, 9003–9012, 1991.
- Chou, M.-D. and M. J. Suarez, An efficient thermal infrared radiation parameterization for use in general circulation models, *NASA Tech. Memo. 104606*, 85 pp., 1994.
- Chou, M.-D., W. L. Ridgway, and M. M.-H. Yan, One-parameter scaling and exponential sum fitting for water vapor and CO₂ infrared transmission functions, *J. Atmos. Sci.*, 50, 2294–2303, 1993.
- Clough, S. A., and M. J. Iacono, Line-by-line calculation of atmospheric fluxes and cooling rates, 2, Application to carbon dioxide, ozone, methane, nitrous oxide, and the halocarbons, *J. Geophys. Res.*, 100, 16,519–16,535, 1995.
- Ellingson, R. G., J. Ellis, and S. Fels, The intercomparison of radiation codes used in climate models: Long wave results, *J. Geophys. Res.*, 96, 8929–8953, 1991.
- Fels, S. B., and M. D. Schwarzkopf, An efficient, accurate algorithm for calculating CO₂ 15 μ m band cooling rates, *J. Geophys. Res.*, 86, 1205–1232, 1981.
- Fu, Q., and K. N. Liou, On the correlated k -distribution method for radiative transfer in nonhomogeneous atmospheres, *J. Atmos. Sci.*, 49, 2139–2156, 1992.
- Goody, R. M., and Y. L. Yung, *Atmospheric Radiation, Theoretical Basis*, 519 pp., Oxford Univ. Press, New York, 1989.
- Intergovernmental Panel on Climate Change (IPCC), *Climate Change, 1994: Radiative Forcing of Climate Change and an Evaluation of the IPCC IS92 Emission Scenarios*, 339 pp., Cambridge Univ. Press, New York, 1995.
- Kiehl, J. T., and B. P. Briegleb, The radiative roles of sulfate aerosols and greenhouse gases in climate forcing, *Science*, 260, 311–314, 1993.
- Kratz, D. P., The correlated k distribution technique as applied to the AVHRR channels, *J. Quant. Spectrosc. Radiat. Transfer*, 53, 501–517, 1995.
- Kratz, D. P., and P. Varanasi, A reexamination of the greenhouse effect due to CFC-11 and CFC-12, *J. Quant. Spectrosc. Radiat. Transfer*, 48, 245–254, 1992.
- Kratz, D. P., M.-D. Chou, and M. M.-H. Yan, Infrared radiation parameterizations for the minor CO₂ bands and for several CFC bands in the window region, *J. Clim.*, 6, 1269–1281, 1993.
- Lacis, A. A., and V. Oinas, A description of the correlated k distribution method for modeling nongray gaseous absorption, thermal emission, and multiple scattering in vertically inhomogeneous atmospheres, *J. Geophys. Res.*, 96, 9027–9063, 1991.
- McClatchey, R. A., R. W. Fenn, J. E. Selby, F. E. Volz, and J. S. Garing, *Optical Properties of the Atmosphere*, 3rd ed., AFCRL-72-0497, *Environ. Res. Pap.* 411, 103 pp., Air Force Cambridge Res. Lab., Bedford, Mass., 1972.
- Penner, S. S., *Quantitative Molecular Spectroscopy and Gas Emissivities*, 587 pp., Addison-Wesley, Reading, Mass., 1959.
- Prabhakara, C., D. P. Kratz, J.-M. Yoo, G. Dalu, and A. Vernekar, Optically thin cirrus clouds: Radiative impact on the warm pool, *J. Quant. Spectrosc. Radiat. Transfer*, 49, 467–483, 1993.
- Rothman, L. S., et al., The HITRAN molecular database editions of 1991 and 1992, *J. Quant. Spectrosc. Radiat. Transfer*, 48, 469–507, 1992.
- Shi, G., and X. Fan, Past, present and future climatic forcing due to greenhouse gases, *Adv. Atmos. Sci.*, 9, 279–286, 1992.
- Stackhouse, P. W., and G. Stephens, A theoretical and observational study of the radiative properties of cirrus: Results from FIRE 1986, *J. Atmos. Sci.*, 48, 2044–2059, 1991.
- Varanasi, P., Absorption coefficients of CFC-11 and CFC-12 needed for atmospheric remote sensing and global warming studies, *J. Quant. Spectrosc. Radiat. Transfer*, 48, 205–219, 1992a.
- Varanasi, P., Absorption spectra of HCFC-22 around 829 cm⁻¹ at atmospheric conditions, *J. Quant. Spectrosc. Radiat. Transfer*, 47, 251–255, 1992b.
- Wang, W.-C., M. P. Dudek, X.-Z. Liang, and J. T. Kiehl, Inadequacy of effective CO₂ as a proxy in simulating the greenhouse effect of other radiatively active gases, *Nature*, 350, 573–577, 1991.

M.-D. Chou, Laboratory for Atmospheres, NASA Goddard Space Flight Center, Greenbelt, MD 20771-0000 (e-mail: chou@climate.gsfc.nasa.gov).

C.-H. Ho, Department of Atmospheric Sciences, Seoul National University, Seoul, 151-742 Korea (e-mail: hoch@climate.snu.ac.kr).

D. P. Kratz, Atmospheric Sciences Division, NASA Langley Research Center, Hampton, VA 23681-2199 (e-mail: d.p.kratz@larc.nasa.gov).

M. M.-H. Yan, Science Systems & Application, Inc., Seabrook, Maryland 20706-2925 (e-mail: yan@climate.gsfc.nasa.gov).

(Received February 28, 1998; revised August 14, 1998; accepted August 19, 1998.)